

Photometric identification of blue horizontal branch stars [★]

K.W. Smith¹, C.A.L. Bailer-Jones¹, R.J. Klement¹, and X.X. Xue²

¹ Max Planck Institute for Astronomy (MPIA), Königstuhl 17, Heidelberg 69117, Germany. e-mail: smith@mpia-hd.mpg.de

² The National Astronomical Observatories, CAS, 20A Datun Road, Chaoyang District, 100012, Beijing, China

Received 9.03.2010; accepted 26.7.2010

ABSTRACT

We investigate the performance of some common machine learning techniques in identifying Blue Horizontal Branch (BHB) stars from photometric data. To train the machine learning algorithms, we use previously published spectroscopic identifications of BHB stars from Sloan Digital Sky Survey (SDSS) data. We investigate the performance of three different techniques, namely *k* nearest neighbour classification, kernel density estimation for discriminant analysis and a support vector machine (SVM). We discuss the performance of the methods in terms of both completeness (what fraction of input BHB stars are successfully returned as BHB stars) and contamination (what fraction of contaminating sources end up in the output BHB sample). We discuss the prospect of trading off these values, achieving lower contamination at the expense of lower completeness, by adjusting probability thresholds for the classification. We also discuss the role of prior probabilities in the classification performance, and we assess via simulations the reliability of the dataset used for training. Overall it seems that no-prior gives the best completeness, but adopting a prior lowers the contamination. We find that the support vector machine generally delivers the lowest contamination for a given level of completeness, and so is our method of choice. Finally, we classify a large sample of SDSS Data Release 7 (DR7) photometry using the SVM trained on the spectroscopic sample. We identify 27,074 probable BHB stars out of a sample of 294,652 stars. We derive photometric parallaxes and demonstrate that our results are reasonable by comparing to known distances for a selection of globular clusters. We attach our classifications, including probabilities, as an electronic table, so that they can be used either directly as a BHB star catalogue, or as priors to a spectroscopic or other classification method. We also provide our final models so that they can be directly applied to new data.

Key words. BHB stars – machine learning – classification

1. Introduction

The blue horizontal branch (BHB) stars are old, metal-poor halo stars. They are of interest as tracers of Galactic structure because they are more luminous than most giant branch or population II main sequence stars, have a narrow range of intrinsic luminosities (hence 'horizontal branch') and display spectral features rendering them identifiable, in particular a strong Balmer jump and narrow strong Balmer lines. There is therefore an interest in building large, reliable samples of them, particularly in the context of wide-field halo surveys such as the Sloan digital sky survey (SDSS) and the forthcoming Pan-Starrs survey. BHB stars are always of interest whenever halo structure is studied due to their strength as distance indicators. Recent studies which have concentrated on BHB stars to trace structure include Harrigan et al. (2010), who searched for moving groups in the halo, Xue et al. (2009) who used them to search for close pairs, implying the existence of halo substructure, Kinman et al. (2009) who searched for a population of BHB stars associated with the thick disk, and Ruhland et al. (2010), who investigated structure in the Sagittarius dwarf and streams. The main problem with BHBs as tracers is their relative sparseness compared to other tracers such as turnoff stars. This means that large, pure samples are highly desirable for structure tracing studies.

In this paper, we take as our lead several recent studies of BHB spectra from SDSS/SEGUE and attempt to use the reliable and large samples of BHBs detected as a training set to build

models aimed at identifying BHBs from the photometry alone. With this tool, we hope to be able to extend the available sample of known (or better, strongly suspected) BHB stars from SDSS and other surveys, with a view either to use our sample directly to trace structure, or at least to guide follow-up studies with spectra.

The main three studies we follow are those of Yanny et al. (2000), who identified a colour cut in the *u-g*, *g-r* colour-colour diagram that yields most of the available BHB population, Sirko et al. (2004) who used spectra to identify a reliable sample of 700-1000 BHBs (the size of the sample depends on the *g* magnitude and the reliability desired), and most importantly Xue et al. (2008), who analysed a sample of SDSS DR6 data using similar techniques to Sirko et al. and extended the reliable list of BHBs to over 2,500 objects. The method of Xue et al. is discussed in more detail in Sect. 3.3.

We have selected three machine learning methods to investigate. These are a *k*-Nearest Neighbour (*k*NN) technique, a kernel density estimator (KDE) and a support vector machine (SVM). We also apply the decision boundary in (*u* - *g*, *g* - *r*) colour space suggested by Yanny et al. (2000) for comparison. After the colour cut, the *k*NN method is probably the simplest algorithm we consider. One example of its use can be found in Marengo & Sanchez (2009). Examples of KDE use in classification problems in astrophysics include Gao et al. (2008), Richards et al. (2009b), Richards et al. (2009a) and Ruhland et al. (2010). The SVM works by identifying a decision boundary in a multidimensional space (Vapnik 1995) (in this case the space of SDSS colours) based on a training set containing examples of two or more classes of object

[★] Tables 7, A.3 and A.4 are only available in electronic form at the CDS via anonymous ftp to cdsarc.u-strasbg.fr (130.79.128.5) or via <http://cdsweb.u-strasbg.fr/cgi-bin/qcat?J/A+A/>

– for our purposes BHB stars and non-BHB contaminants. The SVM performance should be equivalent to that obtainable with a neural network, but it has the advantage of being highly adaptable and relatively easy to use. Its main drawback is its inability to provide genuine probability estimates for classes, because it does not model the distribution of the data. This is discussed further in Sect. 4.4. SVMs have been used on classification problems by various authors, for example Tsalmanza et al. (2007, 2009) who developed a galaxy library for the Gaia mission and explored classification problems therein, Gao et al. (2008) who used them to search for quasars in SDSS data, and Huertas-Company et al. (2009) who used them for morphological galaxy classification. Bailer-Jones et al. (2008) discussed SVM classification of astrophysical sources in the context of unbalanced samples.

We proceed by taking the sample of Xue et al. and obtaining the up-to-date photometry for it from SDSS DR7. We then investigate the ability of each of the three techniques to recover the BHB stars from the Xue sample, and the various options that are available to optimize them. Finally, we take a new sample of DR7 photometry, for sources without spectra, and apply our models to this sample to recover samples of probable BHB stars. We use a selection of globular clusters of known distance to test the BHB classifications and photometric parallaxes.

2. Data

The latest publicly available SDSS data release, DR7, covers approximately 8400 square degrees, with images in the five SDSS bands: u, g, r, i, z . Spectra are available for a subset of the detected objects based on various selection criteria.

The study of Xue et al. used a sample of SDSS DR6 data selected to lie inside the colour box suggested by Yanny et al. (2000) ($0.8 < u - g < 1.6, -0.5 < g - r < 0.0$). We have recovered the sources used by Xue et al. in the DR7 release by matching the SDSS MJD, plateId and fiberId fields. We obtained the PSF magnitudes, estimated extinction, and the parameters (T_{eff} , $\log g$, and $[\text{Fe}/\text{H}]$) as determined by the SDSS pipeline. The dereddened magnitudes were obtained from the model magnitudes during the pipeline processing by applying extinction corrections derived from the map of Schlegel et al. (1998). We recover the extinction from the model magnitudes and apply it to the PSF magnitudes. The DR7 photometry is generally consistent with the DR6 photometry given by Xue et al. to within hundredths of a magnitude, but there are a number of sources with more divergent values. We rejected the most discrepant of these by introducing a colour cut 0.1 magnitudes outside of the colour cut of Yanny et al.. This cut excluded mostly contaminant stars. The Xue et al. sample contained 10224 objects, of which 2558 were identified by them as BHB stars. After rejecting sources with discrepant photometry, 9929 objects remained, of which 2536 were identified by Xue et al. as BHB stars.

We also cross matched against a list of 1172 objects from the paper of Sirko et al.. All these objects were identified by Sirko et al. as BHB stars. Since Sirko et al. did not provide SDSS identities in their table, we cross matched first with our SDSS data on the basis of RA and Dec and g magnitude. After cross matching, 1101 of the sources were identified in the SDSS DR7 data. Of these, 4 had no identified counterpart amongst the Xue et al. objects. Figure 1 shows the colour-colour diagram of our sample.

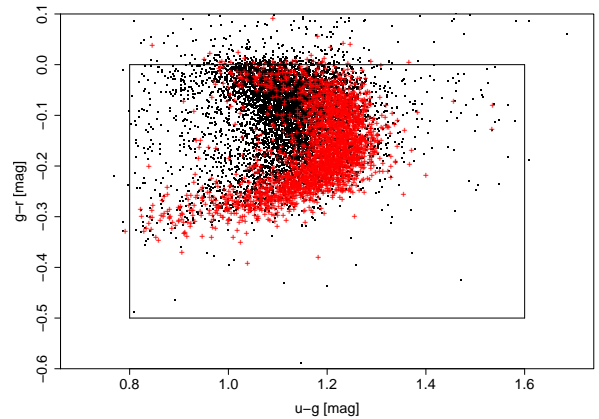


Fig. 1. The sample of Xue et al. (2008) in the $u - g, g - r$ plane, with DR7 data. BHB stars (according to Xue et al.) are shown as red crosses, non-BHB stars as black points. The box shows the colour cut used by Xue et al. (2008) and Yanny et al. (2000). The outer boundary extends 0.1 magnitudes beyond this. Sources outside the plot region were discarded.

3. General Approach

All our classification methods are supervised, meaning that they require samples of data for objects of known type in order to train a model, which can then be applied to new data. Various parameters must be set to optimize the classification, and in the end the reliability of the methods relative to each other and in absolute terms has to be determined in some way. For these reasons, we need a sample of test objects of known type on which we can run our trained models. Our sample contains 2536 BHB stars as identified by Xue et al. Our standard procedure was to randomly split the BHB sources into roughly equal training and testing sets, and then randomly select equal numbers of non-BHB sources (designated “other”) to include in the training and testing samples. We can investigate the statistical properties of the results by bootstrapping.

3.1. Data dimensionality and feature selection

The PSF photometry was corrected for the expected extinction determined by the SDSS pipeline. There are four colours available. The $u - g$ and $g - r$ colours are the most important for BHBs. The others show little or no real information when examined by eye. They make some difference (for the better) for the kNN and SVM methods, but tend to degrade the KDE. It is possible that the improvement seen for kNN and SVM by including the other colours is mostly due to excluding faint sources due to their large scatter in all bands.

3.2. Comparing methods: completeness and contamination

The *completeness* is defined as the number of correctly classified sources of a particular class, divided by the number of available sources of that class, i.e. it is the fraction of test sources of a particular class that are correctly classified,

$$\text{completeness}_j = \frac{n_{i=j,j}}{N_i}, \quad (1)$$

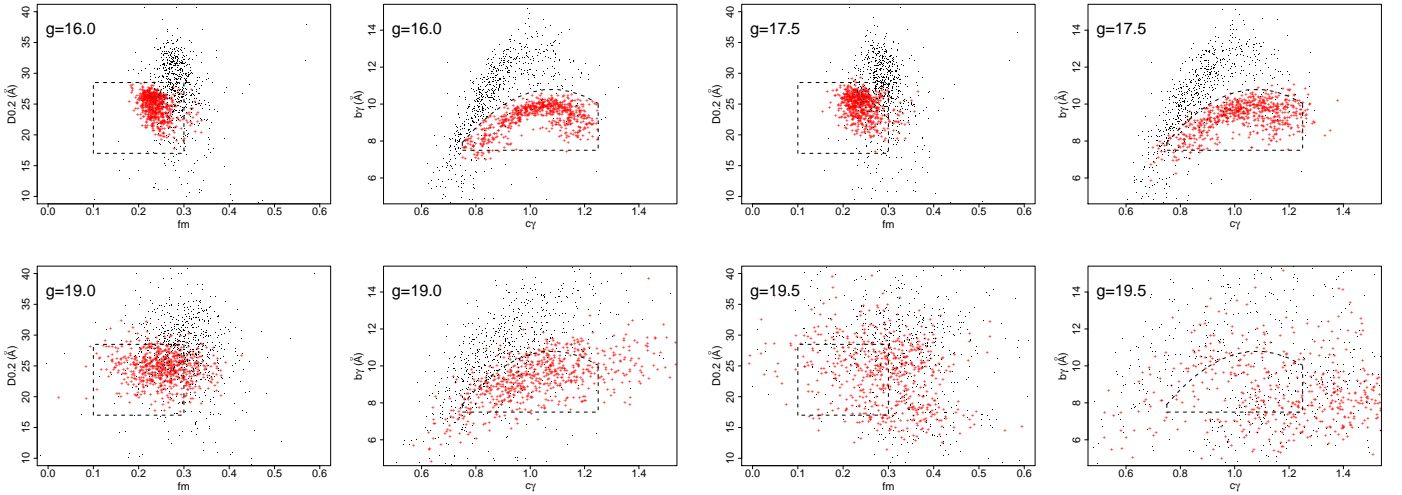


Fig. 2. Simulation of the effect of noise on Xue et al.’s classification. The four spectral line parameters used in the classification are fm , $D0.2$, c_γ , and b_γ (see Xue et al. (2008) for details). Four magnitudes are illustrated, for each of these, we plot $D0.2$ versus fm and c_γ versus b_γ . The selection boxes are shown in each panel. The progressive loss of BHB stars (red crosses) from the selection box is clear. Non-BHB stars (black dots) are not scattered into the boxes at the same rate.

where $n_{i,j}$ is the number of objects of true class i classified as output class j and N_i is the total number of input sources of class i . Input sources can be lost from the output class due to misclassification into another class, or by remaining unclassified due to an insufficiently high classification confidence. The *contamination* of the output sample is defined as the number of falsely classified sources of that class divided by the number of sources classified into that class, whether correctly or incorrectly,

$$\text{contamination}_j = \frac{\sum_{i \neq j} n_{i,j}}{\sum_i n_{i,j}}, \quad (2)$$

In our particular case, one class, the set of non-BHB stars, is really a mixed class of contaminants comprising blue stragglers and main sequence stars, that we are interested in removing in order to obtain a clean sample of BHB stars. Therefore, we are interested in the completeness and contamination of the BHB sample and not primarily in the completeness or contamination of the “other” class.

3.3. Reliability of the training and testing sets

Since our method is based on the results of Xue et al., it is worthwhile investigating how reliable these are, particularly at the faint end. To this end, we selected 1381 spectra from Xue et al.’s original data, having $14.5 < g < 15.5$. Roughly half of these (655) were BHB stars. We then added artificial noise to degrade them to the same signal-to-noise ratio as fainter spectra. We constructed in this way eight artificial samples in half magnitude steps from $g=16.0$ to $g=19.5$. We then reanalysed these degraded spectra with the technique of Xue et al. and reclassified them. We then compare the performance at faint magnitudes with the original performance.

The classification of Xue et al. is based on recovering four different characteristic parameters from the absorption lines. These are $D0.2$, the width at 20% below the continuum of the Balmer line, fm , the flux relative to the continuum at the line core, and c_γ and b_γ , which are parameters from a Sérsic fit to the line shape (Sérsic 1968). BHB stars are identified as lying

within selection boxes in the feature space formed by the line parameters. This selection is illustrated for our degraded data in Fig. 2, which shows for four example magnitudes the $D0.2$ versus fm and c_γ versus b_γ values, and the selection boxes. It is clear from the figure that, as the noise increases, true BHB stars scatter outside one or the other selection box and are lost, decreasing the completeness. Some sources from outside the selection boxes scatter into the box, but since the box covers a small fraction of the data space, and since a contaminant has to scatter into both boxes to be misclassified as a BHB, the increase in the absolute number of contaminating sources is modest. The contamination, as defined above, will still increase because the number of true positives, in the denominator of Equation 2, is decreasing. Figure 3 shows the resulting ratio of objects classified (rightly or wrongly) as BHB stars to total stars as a function of g . This is discussed in terms of the effect on the prior probability in the following section. For now, we note that this effect kicks in strongly for sources fainter than $g=19.0$, and that it will degrade the quality of training sets used to define models and also of any testing set used to assess them.

3.4. Priors

The classifiers we use are trained on mixed samples of BHB and non-BHB stars with a range of properties. We implicitly assume that the classifier takes account of the likely distribution of the population of objects to be classified, and if it does not, we need to correct the classifier output probabilities using appropriate priors.

The simplest prior to be accounted for is the true class fraction. To train our models, we use equal numbers of BHB and non-BHB stars, whereas the true class fractions are not equal (the fraction of BHB stars in the sample of Xue et al. is approximately 0.26 for all sources). For the kNN and KDE methods we could directly include the class fractions in the training sets. For the SVM we could also include proportional fractions of classes, but the actual effect of this on the classifier is complex and not well understood. We choose to always use equal class fractions

and use a prior to adjust the classifier output. We refer to this type of class fraction prior as a 'simple prior' hereafter.

We can also adjust for prior probabilities as a function of other parameters that are not accounted for by the classifier itself. We consider g magnitude and b , the Galactic latitude. In Fig. 4 we show the ratio of the density functions of BHB stars and all stars as functions of g in the sample of Xue et al. (dashed green line). Because these density functions were individually normalized, the resulting ratio is the relative fraction of BHB stars, rather than the absolute fraction - i.e. it is as if the class fractions were equal.

Also shown in this plot is the ratio of BHB stars to all sources at each magnitude as estimated from the experiment described above in Sect. 3.3 (red dash-dotted line). This curve, which is a renormalized version of the curve shown in Fig. 3, shows what we would expect to see if the fraction of BHB stars in the true population was constant with g , but the observed ratio was altered by sources being lost due to increasing noise at high magnitudes. We can correct the measured ratio of BHBs to all sources for this effect. This correction mitigates the falloff of the ratio at the faint end. The corrected curve is shown as the dotted blue line. We use this as the basis of the magnitude dependent prior, but the correction causes a spike at the faint end that is probably due to small numbers of sources and is obviously not desirable in the prior. For this reason we have truncated the function before it turns up and adopted a plateau for the high magnitude end. Similarly, we adopt a plateau at the bright end, where the fraction may be strongly affected by the SDSS spectrum selection function (there is a cutoff at $g < 14$ for the Legacy spectra, (Adelman-McCarthy et al. 2006)). The adopted prior as a function of g is plotted as the solid black line in Fig. 4.

Figure 5 shows the ratio of density functions for BHB and non-BHB sources as a function of absolute Galactic latitude. This ratio shows a relatively smooth trend, with quite a lot of structure superimposed. We model it with a straight line fit and adopt this fit as the relative prior in latitude.

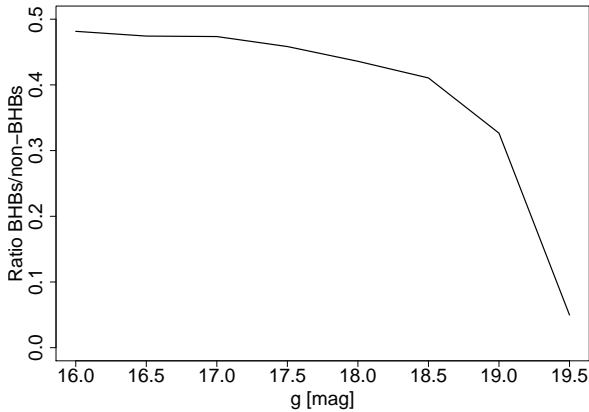


Fig. 3. The effect of increasing noise on the spectroscopic classification of Xue et al., as illustrated in Fig. 2. The line shows the ratio of the number of *output* BHB stars, that is, the sources classified as BHB stars, regardless of whether they really are or not, to total stars.

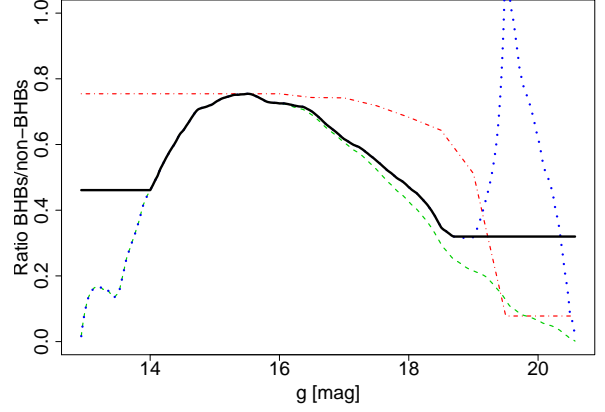


Fig. 4. The dashed green line shows the ratio of the density function of BHB stars to the density function of all stars. The dot-dashed red line shows the ratio of BHB stars to non-BHB stars from the classification described in Sect. 3.3. This is the same curve plotted in Fig. 3 but it has been renormalized so that the peak is at the same level as the peak of the ratio of density functions - i.e. so that it doesn't include the simple prior. The dotted blue curve is the result of correcting the basic BHB fraction (dashed green line) for the expected change in the ratio due to noisy spectra. The regions at either end are replaced with a constant value, and the prior actually adopted is plotted as the thick solid black line.

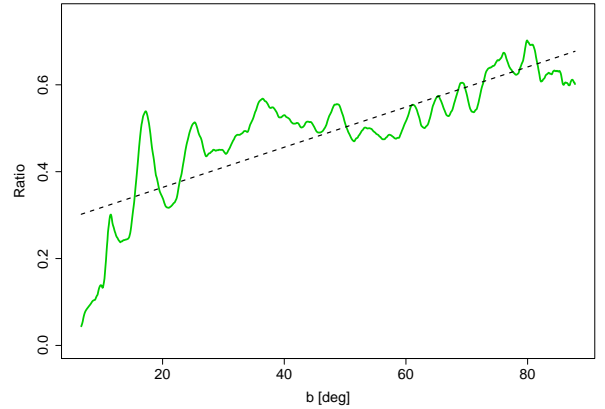


Fig. 5. The solid green line shows the ratio of BHB star density to the sum of BHB density and other stars density as a function of galactic latitude b . The dashed black line is a linear fit used to build the 2-dimensional prior as described in the text.

If these priors are independent of one another, we can apply them in sequence to the output posterior probability of the classifier using

$$P(C|D_1, D_2, \dots, D_N) = \prod_{n=1}^N \frac{P(C|D_n)}{P(C)^{N-1}}, \quad (3)$$

where $P(C|D_n)$ is the probability of class membership given some piece of information, D_n . This formula is discussed in depth in Bailer-Jones & Smith (2010). The issue of class fraction priors and its influence on classifier training is discussed in Bailer-Jones et al. (2008). The correlation of g and b is low, with a Pearson coefficient of -0.0017. The assumption of independence therefore holds well.

The ratio of BHB stars to all stars for all data is 0.26, however this includes regions where the selection function for SDSS spectra has a large effect (there is a cutoff at $g = 14$ for SDSS Legacy spectra and g, r or $i=15$ for SEGUE, and at $g > 19$ the reliability of the Xue et al. classification method becomes difficult to assess). The ratio of BHB stars to all stars in the interval $14 < g < 19$ is 0.32. We use this latter fraction as the class fraction.

For the analysis of the different classifiers, we consider two different priors, a simple ratio (equal to 0.32) that represents the fraction of BHB stars to all stars over the sample in the interval $14 < g < 19$, and the combination of this with the priors as functions of g or b as discussed above. We refer to the first prior as a 'simple prior' and to the second as a '2d prior', because it is a function of the two variables g and b .

3.5. Priors and performance measures

The issue of the class fractions enters the analysis in two distinct ways, and it is worth discussing this issue explicitly because it can easily lead to confusion.

Firstly, the class fractions are the single most important contribution to the prior probability used to obtain posterior probabilities for each object. This issue is reasonably clear.

Secondly, as well as adjusting the classifier probabilities with the prior, when testing the classifiers, we **also** have to take account of the uneven expected class fractions in the measured contamination (and in any other quantity where they would be important – the completeness is not affected, as can be seen from Equation 1). We can do this by either using a test set that reflects the true expected fractions (which would be possible in our case because the classes are not extremely unbalanced), or by correcting the contamination for the difference between the input test set fractions and the expected true fractions. Since the population composition as a function of g and b is already present in the test set, no correction should be made to the test output to correct for the relative fractions of BHB stars as a function of these quantities.

Note that this reweighting of the contaminants in the output sample has to be carried out anyway if the expected class fractions are different to the fractions in the test set, whether or not we also apply the prior to the classifier probabilities. All the contaminations presented in this paper, except that in Table 2, are based on test sets with equal class fractions, and are corrected to the expected class fractions after the classification using the estimated fraction of 32% BHB stars.

The issue of priors in the context of a classification problem with a highly unbalanced data set was addressed in some depth by Bailer-Jones et al. (2008). In particular, Sect. 2.5.1 of this paper discusses the issue of correction of the contamination

Table 1. Coefficients for decision boundary in $u - g, g - r$.

Segment	m	c
$-0.3 < g - r \leq -0.25$	2.4	1.62
$-0.25 < g - r \leq -0.15$	1.6	1.42
$-0.15 < g - r \leq 0$	-0.533	1.1

Table 2. Results of classification with decision boundary.

	Absolute	
	bhb	other
BHB	1963	486
OTHER	2560	3321
Unclassified	436	
	Percentage	
	bhb	other
BHB	80.16	19.84
OTHER	43.53	56.47
	Completeness	Contamination
BHB	0.802	0.566

in more depth than is possible here. There the specific problem was identifying quasars amongst stellar samples, which is an extremely unbalanced problem. The issue with BHB stars is less severe.

4. Comparative performance of machine learning techniques

4.1. Colour box and direct decision boundary

Yanny et al. (2000) derived a decision boundary in $u - g, g - r$ colour space to distinguish low gravity BHB giants from contaminating MS and BS stars in the colour box. Their decision boundary consists of three straight line segments and is shown in their Fig. 10. Our estimates of the gradients and intercepts of the line segments are shown in Table 1. Sources are BHB stars if they have $u - g < m(g - r) + c$, with values of m and c taken from the Table.

We classified our test set with this boundary, and obtained the results summarized in Table 2. All sources with $g < 19$ were classified, since no training set is needed. The test set class fractions are not artificially balanced, so no prior has been applied. Sources lying outside the ranges of Table 1 remain unclassified. The results are presented first in the form of a confusion matrix. Each row of the matrix corresponds to a particular true class, either BHB or other. The rows are labeled in capitals to indicate that this is the true class of the object. The columns list the output classifications. The leading diagonal of the matrix therefore shows the true classifications. The off diagonal elements indicate misclassifications, and it is possible to see which classes are particularly confused with one another. The confusion matrix is presented twice, once with the absolute numbers of objects in each classification bin, and once with the classifications expressed as percentages of the total number of input objects of that class. The rows of this matrix therefore sum to one. We also present the completeness and contamination obtained with this method.

4.2. k -Nearest Neighbours

Nearest neighbour techniques are probably the simplest and most intuitively obvious method for supervised classification. For a given new object, we select the k nearest training points in the data space and assign a class based on the classes of the neighbours. For $k > 1$ we could choose to select a simple ma-

jority of objects, or we could impose a higher threshold in an attempt to improve the purity of one or both of the output classes (i.e. BHB stars or other). Introducing a threshold implies that we must be prepared to tolerate non-classifications.

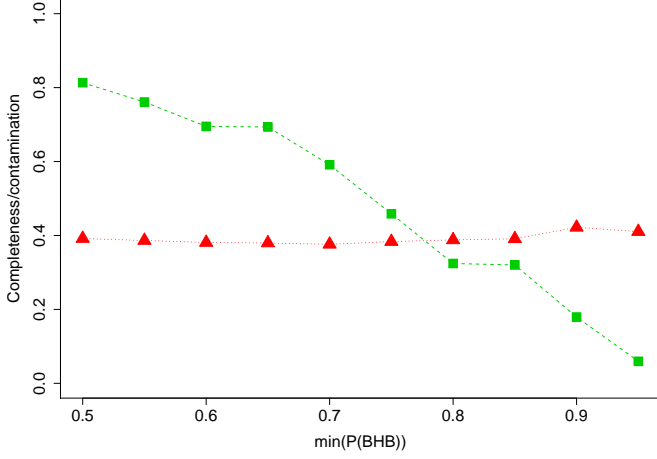


Fig. 6. The effect on the completeness (green squares) and contamination (red triangles) of varying the minimum probability (including the effect of the 2d prior) required for a positive classification in the kNN method. The completeness (necessarily) falls as the threshold is increased.

A probability can be estimated from the fraction of neighbours belonging to each class, so for example if nine out of ten of the nearest neighbours are BHB stars, we would estimate $P(BHB) = 0.9$.

We ran the kNN technique for various choices of k and measured the output sample completeness and contamination. The classifier was run with ten resamplings of the training and test sets for each k , from $k = 1$ up to $k = 100$, and the classification was performed with simple majority voting. The completeness was found to be approximately constant with increasing k , but the contamination showed a shallow minimum at around $k = 15$, which we selected as the optimum value.

We also experimented by cutting the colours used from four down to two ($u - g$ and $g - r$). The result was a slight degrading of the results for all values of k . We therefore use the kNN technique with the four dereddened colours.

We next investigated the effect of varying the confidence threshold for classification and measuring the completeness and contamination of the output BHB star sample. Increasing the threshold would be expected to lead to a loss of completeness, but also a lowering of the contamination. The results of this for kNN are shown in Fig. 6. The completeness does indeed fall, but the contamination remains constant at around 0.4.

We performed ten classifications, with resampled training and testing sets, with the kNN method to get a final estimate of performance. The value of k and the probability threshold were left fixed ($k = 15$, threshold=0.5). The results are shown in Table 3. This table is divided into three sections. In the top section, we present the results of applying the classifier to the test data without applying any prior. This is equivalent to assuming equal true class fractions. The second section presents the results with the application of the so-called simple prior, with which we

Table 3. Results for kNN classification.

With equal priors		
	Absolute	
	bhb	other
BHB	1008	235
OTHER	347	871
	Percentage	
BHB	81.09	18.91
OTHER	28.49	71.51
	Completeness	Contamination
BHB	0.811	0.422
With simple prior		
	Absolute	
	bhb	other
BHB	743	500
OTHER	245	973
	Percentage	
BHB	59.77	40.23
OTHER	20.11	79.89
	Completeness	Contamination
BHB	0.598	0.412
With 2d prior		
	Absolute	
	bhb	other
BHB	920	323
OTHER	264	954
	Percentage	
BHB	74.01	25.99
OTHER	21.67	78.33
	Completeness	Contamination
BHB	0.740	0.378

Notes. *Top section:* Confusion matrix showing the results of kNN classification ($k=15$) with threshold $P(BHB) > 0.5$. This is the combined result of ten independent classifications with resampling of the training and testing sets. The rows show the true class (according to Xue et al.), the columns show the classifier output class. When shown as percentages, the quantities in the rows should add to 100%, but the quantities in the columns in general do not. The completeness and contamination are also shown - and the contamination is corrected for the class imbalance using the simple prior. *Middle section:* The same confusion matrix, with output probabilities corrected for the simple prior. *Bottom section:* The results with output probabilities corrected for the prior probability as function of g magnitude and galactic latitude.

correct for the effect of the class fractions only. The final section presents the results with the application of the 2d prior, a function of g and l . In each section we present the results as confusion matrices of absolute classifications and as percentages of the input true classes. Finally we present the completeness and contamination.

Figure 7 shows the completeness and contamination for test samples classified with the kNN method, with the results binned by magnitude. The threshold for classification is always 0.5, and $k=15$. This is the average of 100 separate trials. The lower plot shows the standard deviation in each bin.

As expected, the classifier performance falls off for fainter magnitudes. Part of this effect may be due to the natural confusion in the test set between BHB stars and non-BHB stars, introduced by the noise in the method of Xue et al. (2008).

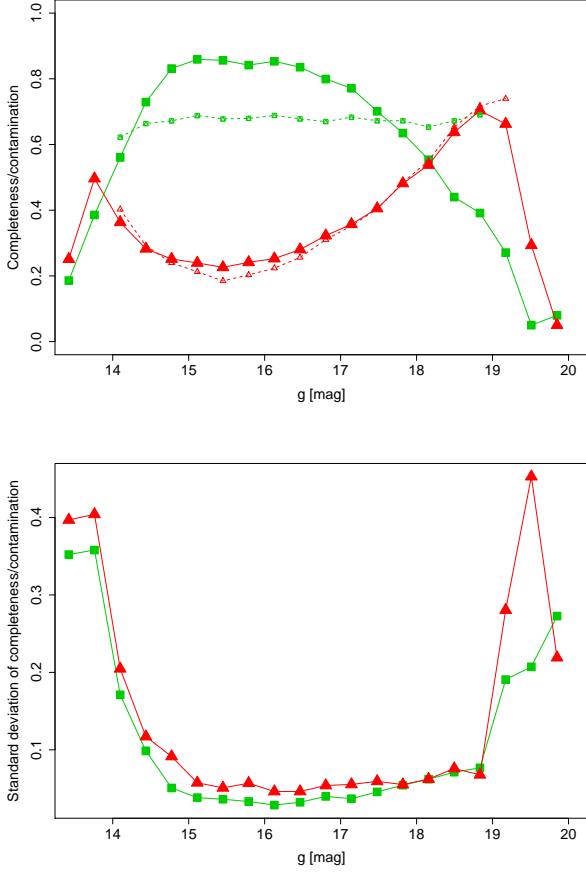


Fig. 7. *Top:* Completeness (green squares) and contamination (red triangles) for sources of different magnitudes classified with the kNN technique. One hundred separate trials were averaged to produce this plot. The filled symbols and solid lines show the results using the 2d prior. The open symbols and dashed lines show the results using the simple prior only. *Bottom:* Standard deviations of completeness and contamination at each point.

4.3. Kernel density estimation for classification

We next consider a kernel density estimation (KDE) approach to the classification. The density estimate is a weighted mean of neighbours, the weighting function being a kernel of choice. See Hastie et al. (2001) for a general discussion of the method, and see Richards et al. (2009a,b) for examples of KDE used to identify quasars in SDSS data.

We use an Epanechnikov kernel, which is truncated and so is less influenced by distant points. In practice, the choice of kernel is usually less important than the bandwidth value. The bandwidth was set independently for each dimension. The package *np* in R* was used to implement the KDE method (Hayfield & Racine 2008), and also to determine the optimal value for the bandwidth, using the method of Li & Racine (2003). This is based on leave one-out-cross validation and involves minimizing the variance amongst trial density functions constructed with different bandwidth values.

Trial and error experimentation with the available colours shows that reasonable results can be obtained with $u-g$ and $g-r$, but the addition of further colours degrades the performance. We

construct density functions for both the BHB stars and the non-BHB stars and compare the values at the locations of test data or new data points to classify the source. The individual density functions for BHB and non-BHB sources in the training set are shown as contours in $u-g$, $g-r$ space in Fig. 8. The probability of an object being of class $c1$ from a number n_c of possible classes is taken to be

$$P(j) = \frac{K_{j=c1}(\mathbf{x})}{\sum_j^{n_c} K_j(\mathbf{x})} \quad (4)$$

where K_j are the density functions for each class and \mathbf{x} are the data.

Training and test sets were independently selected ten times and used to train and test a model. We applied the KDE classifier to the test set under the assumptions of equal class sizes (flat prior), the simple prior ($P(BHB) = 0.32$ for all sources), and the 2d prior. The results for all these tests are shown in Table 4. The layout of this table is the same as Table 3.

As with the kNN method, we experimented with thresholds at different levels of classification confidence. We adjust the threshold probability for BHB classification and record the resulting output sample completeness and the contamination. These are shown in Fig. 9. As expected, the effect of introducing a threshold higher than 0.5 for classification is to reduce both the completeness and contamination.

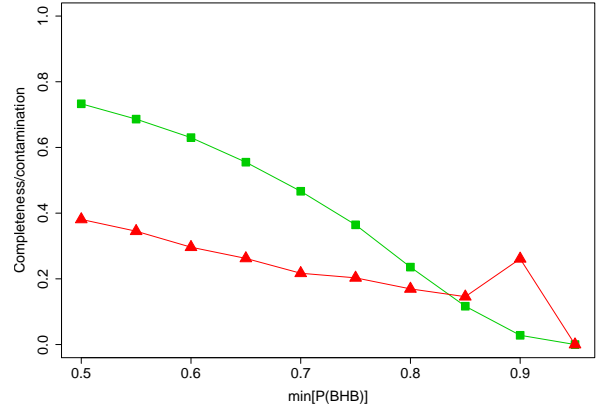


Fig. 9. Effect of varying the probability threshold with the KDE method for classification as a BHB star on the completeness (green squares) and contamination (red triangles) of the output. The results shown in Table 4 correspond to a probability threshold of 0.5. Output probabilities have been modified by the 2d prior.

Figure 10 shows the completeness and contamination for the test sample classified with the KDE method, with the results binned by magnitude. The threshold for classification is always 0.5.

4.4. Support vector classification

Support vector classification is a supervised method in which a high dimensional decision boundary is fit between two classes.

* <http://www.r-project.org>

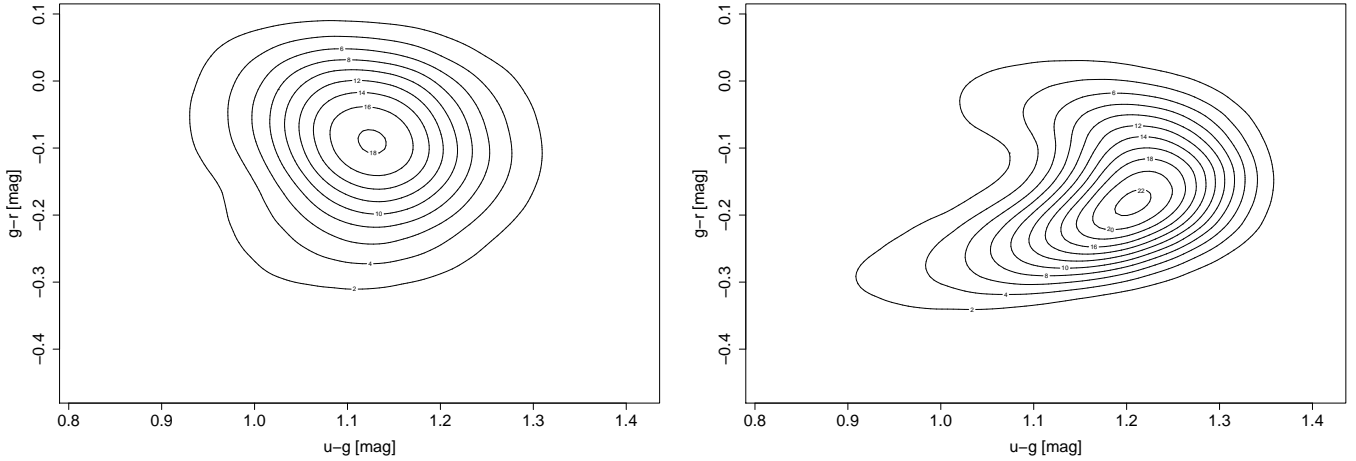


Fig. 8. The density of points for the non-BHB star training set (left) and the BHB star training set (right) in the $u - g$, $g - r$ plane. These density functions are used for the KDE classification. Contours range from 2 to 22 stars per unit area in steps of 2.

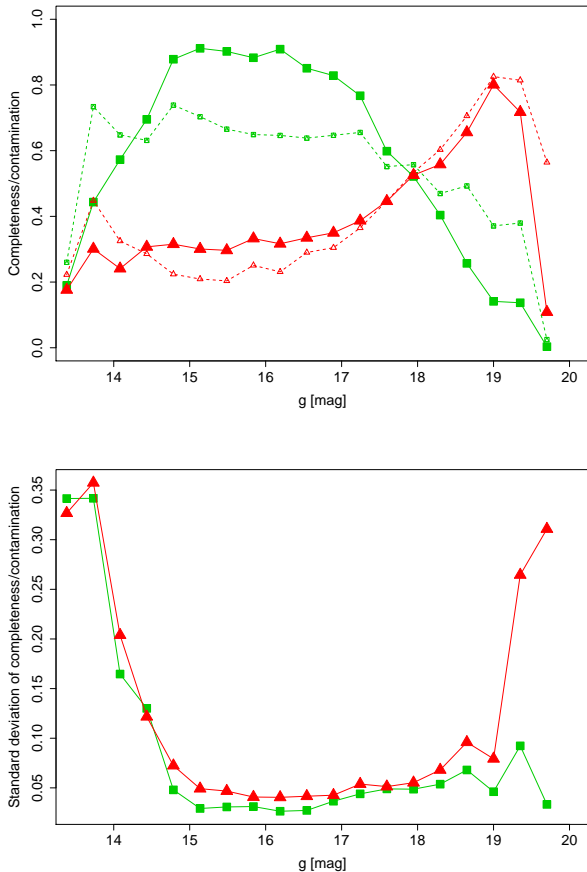


Fig. 10. *Top:* Completeness (green squares) and contamination (red triangles) for sources of different magnitudes classified with the KDE technique with one hundred trials. The filled symbols and solid lines show the results using the 2d prior. The open symbols and dashed lines show the results using the simple prior only. *Bottom:* Standard deviation of completeness and contamination over one hundred trials.

The boundary is chosen to maximize the margins with the nearest representative points of each class (the so-called support vectors). See Vapnik (1995) for a fuller description. A linear SVM defines a boundary that is linear in the original data space (in our case the four SDSS colours). By using a kernel function, a higher dimensional feature space can be defined, and the decision boundary instead defined in this. We use the second order radial basis function as a kernel here. This function has a single parameter, gamma, which must be set before training the model. To deal with the problem of regularization for noisy data, a cost parameter can be introduced, that acts to soften the margin. The cost parameter is so called because it controls the extent to which the algorithm will attempt to fit a more complex boundary in order to correctly classify all of the training points, i.e. it is the 'cost' to the algorithm of misfitting training points during the model training (Cortes & Vapnik 1995). We use the libSvm implementation, which is available online (<http://www.csie.ntu.edu.tw/~cjlin/libsvm/>, Chang & Lin (2001)) and is implemented in the R package e1071.

4.4.1. Probabilities from SVM

The SVM method is not designed to provide probabilities, since it deliberately discards many of the training points, using only the support vectors to build the model of the decision boundary. However, a probability estimate can be made based on the distance of a test point from the decision boundary (Platt 1999). The actual probability returned is based on a model fitted to the training data. This probability estimate is essential if we want to trade off completeness versus contamination, or use priors.

The training data were standardized colour by colour so that each of the colours had zero mean and unit standard deviation. The same offset and scaling, calculated from the training data, were applied to the testing data. The SVM was run over a grid of parameters; cost and gamma, with a fourfold cross validation using the training data to determine the best choice for these values. The optimum values chosen were $\gamma=0.25$, $\text{cost}=64$. The model was then trained on the training set and applied to the test set. The basic classification performance is shown in Table 5.

Table 4. Results for KDE classification.

Equal priors		
	Absolute	
	bhb	other
BHB	1021	222
OTHER	505	713
	Percent	
	bhb	other
BHB	82.1 %	17.9 %
OTHER	41.5 %	58.5 %
	Completeness	Contamination
BHB	0.821	0.512
With simple prior		
	bhb	other
BHB	765	478
OTHER	281	937
	Percent	
	bhb	other
BHB	61.5 %	38.5 %
OTHER	23.1 %	76.9 %
	Completeness	Contamination
BHB	0.615	0.438
With 2d prior		
	bhb	other
BHB	912	331
OTHER	293	925
	Percent	
	bhb	other
BHB	73.4 %	26.6 %
OTHER	24.1 %	75.9 %
	Completeness	Contamination
BHB	0.734	0.405

Notes. *Top section:* Confusion matrix showing results of KDE classification of 10 independently selected test sets based on 10 independently trained models. The classification threshold is $P(BHB) \geq 0.5$ in each case. The results are shown at the top as mean numbers of sources in each category and then as percentages. The completeness and contamination for the BHB output sample is also shown. These are corrected for the expected unbalanced class fractions. *Middle section:* The same quantities calculated with the simple prior applied to the classifier output probabilities. *Bottom section:* The confusion matrix, BHB completeness and BHB contamination obtained when the prior as a function of g and latitude is applied to the classifier output probabilities.

We consider the effect of a threshold on the measured completeness and contamination. The results of introducing various thresholds greater than $P(BHB) = 0.5$ are shown in Fig. 11. It can be seen from Fig. 11 that the completeness and contamination both fall as the threshold is increased, except for very high thresholds when the contamination in fact rises. This is possible if the set of sources with the highest values of $P(BHB)$ contain a large number of contaminants. This is undesirable, but is partly caused by the low number of sources with high $P(BHB)$ - in fact there are only thirteen sources with $P(BHB) > 0.9$.

Figure 12 shows the completeness and contamination for the test sample classified with SVM, with the results binned by magnitude. This plot shows the results both with the simple prior and the 2d prior. As with the KDE method, the SVM performs well for $14 < g < 18$ but progressively more poorly for fainter sources.

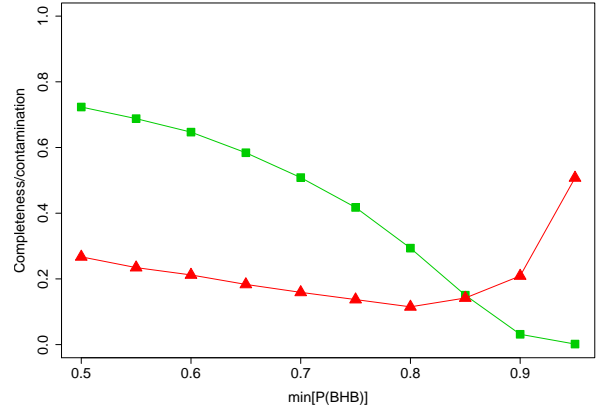
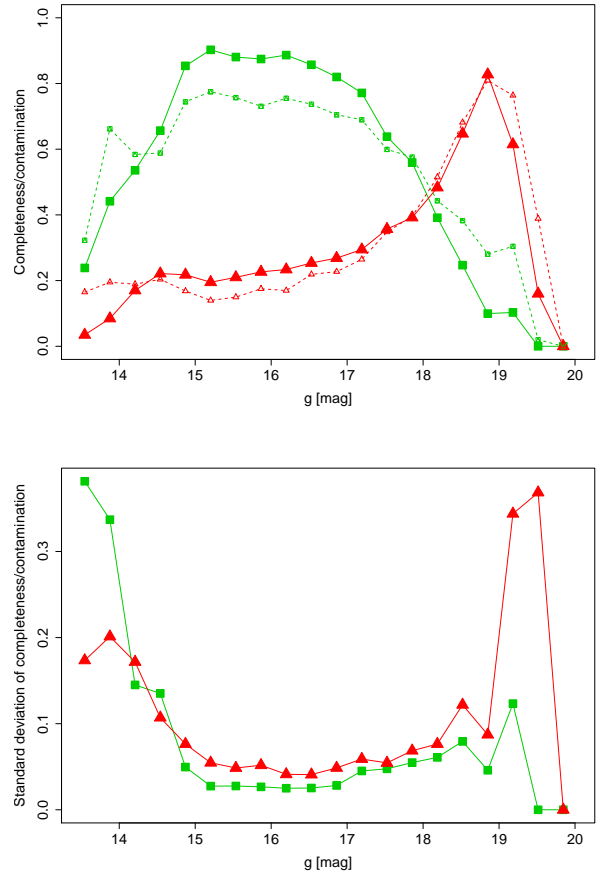

Fig. 11. Plot of completeness (green squares) and contamination (red triangles) as a function of a threshold probability for BHB classification in the case of the SVM classifier. The results shown in Table 5 correspond to a probability threshold of 0.5. Output probabilities have been modified by the 2d prior.

Fig. 12. *Top:* Completeness (green squares) and contamination (red triangles) for sources of different magnitudes classified using SVM with one hundred trials. The filled symbols and solid lines show the results using the 2d prior. The open symbols and dashed lines show the results using the simple prior only. *Bottom:* Standard deviations of one hundred trials.

Table 5. Results for SVM classification.

Flat prior		
	Absolute	
	bhb	other
BHB	988	255
OTHER	305	913
	Percent	
	bhb	other
BHB	79.5%	20.5%
OTHER	25.0%	75.0%
	Completeness	Contamination
BHB	0.795	0.396
Simple prior		
	Absolute	
	bhb	other
BHB	836	407
OTHER	188	1030
	Percent	
	bhb	other
BHB	67.3%	32.7%
OTHER	15.4%	84.6%
	Completeness	Contamination
BHB	0.673	0.323
With 2d prior		
	Absolute	
	bhb	other
BHB	912	331
OTHER	187	1031
	Percent	
	bhb	other
BHB	73.4%	26.6%
OTHER	15.4%	84.6%
	Completeness	Contamination
BHB	0.73	0.303

Notes. *Top section:* Confusion matrix showing results of an SVM classification without priors and with a threshold of $P(BHB) > 0.5$, also the completeness and contamination in the output BHB sample, corrected for the expected class imbalance. *Middle section:* the same quantities obtained applying the simple prior probability for all sources. *Bottom section:* The confusion matrix and completeness and contamination found when applying the prior as a function of g and latitude.

4.5. Optimal choice of classifier

From the bare results in Tables 3, 4 and 5, using the 2d prior, all the techniques have very similar completeness. The contamination is best in the case of SVM with about 0.3, and worst for the KDE with 0.4. The decision boundary method of Yanny et al. (2000) should properly be compared with the simple prior case for the three machine learning methods – the test set naturally has the right class fractions, but because the method is not probabilistic, the correction for the 2d prior cannot be made. The completeness of the decision boundary method is clearly better than the three machine learning methods. The contamination of over 50% is however worse than any of them.

From the magnitude performance plots in Figs. 7, 10 and 12, it can be seen that all the methods achieve a high completeness and low contamination for the approximate range $15 < g < 17$. The contamination achieved by the SVM technique for the region of best performance between $15 < g < 17$ is slightly better than for the kNN.

To make a more direct comparison, we plot in Fig. 13 the completeness and contamination, averaged over ten indepen-

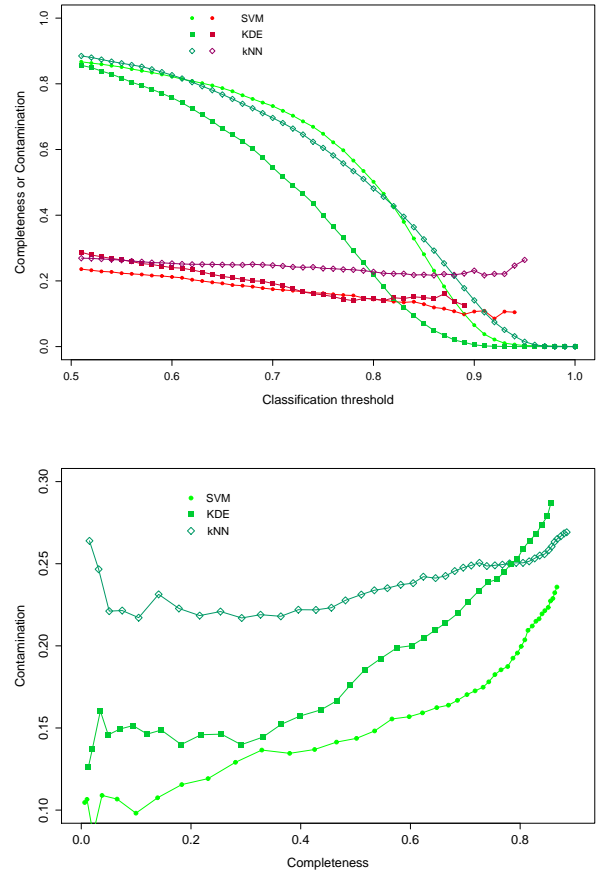


Fig. 13. *Top:* Completeness (green) and contamination (red) for test samples with $15 < g < 17$ classified with the SVM, KDE or kNN. Different shades and symbols are used to distinguish the methods. All results are modified with the 2d prior and the contamination is corrected for class fractions. Results are the average of ten independent runs. *Bottom:* Same data as in the top plot, with completeness plotted directly against contamination for direct comparison. The SVM results are always below and to the right of the other methods, demonstrating lower contamination for a given completeness.

dent trials, for all the methods as a function of the classification threshold. For this plot, we restrict the test sample to sources in the range $15 < g < 17$, where all the methods perform reasonably well.

From this comparison, we can note the following; The SVM and kNN methods deliver similar completeness over most of the range of thresholds. The kNN technique maintains completeness better than SVM for very high thresholds. However, the kNN method does not show any significant improvement in contamination, and it never delivers a better contamination than the other methods for similar completeness. The other techniques do show a falling contamination with increasing threshold. In the lower plot, it is clear that the SVM delivers on average a lower contamination for a given completeness.

In summary, all the methods perform reasonably well, but the SVM seems to have the edge across the largest range of conditions, and we choose to use this technique on the new data.

5. Classification of new data

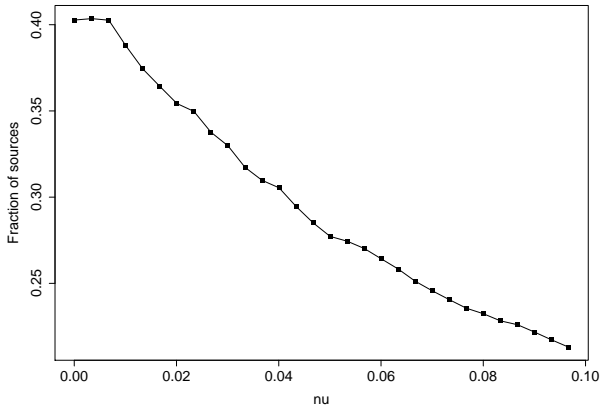


Fig. 14. The fraction of new data points passing through the one class filter as a function of the parameter ν . The higher the value of the parameter, the more objects are rejected, and fewer then remain for the main classification. The fraction reaches a plateau at around $\nu = 0.01$.

We obtained new DR7 photometry from SDSS and use the various models to predict the classes (BHB versus non-BHB). The DR7 data were obtained using the colour cut of Yanny et al. (see Sect. 2). The search yielded 859,341 objects at $g < 23$. This magnitude cutoff is very deep, being 0.8 magnitudes deeper than the 95% completeness limit for DR7 (Abazajain et al. 2009). However, the selection requires good photometry in all five SDSS bands, and the classification method will enforce the condition that classified objects occupy the data space defined by the training set (see next section), so that the number of spurious objects in the sample will eventually be very low.

5.1. One class filter

Before attempting to classify the new data, it is necessary to exclude points which lie outside the locus of the available training points. This issue did not arise when using the testing data as described previously, since all input sources are by definition part of the defined data set and could potentially be used to train a classifier. New points lying in a 'hinterland' outside the training data locus and well away from the decision boundary may be misclassified with high confidence levels, since the probability model is based on distance from the decision boundary. It is necessary to exclude such points prior to attempting the classification.

To do this, we used an SVM in one-class mode. The one-class SVM defines a decision boundary which separates the training data from the origin with a maximized margin. A parameter, ν , controls the rigidity of the boundary, and hence what fraction of the training set would typically be excluded. We collected all the available training objects (2,536 BHBs and 7,511 non-BHBs) together into one set and standardized according to this data. We conducted an experiment with different values of the parameter ν to see how many of the new data points would pass through. The results are shown in Fig. 14. From this figure, we see that the fraction of sources passing through the filter reaches a plateau for values of ν a little less than 0.01. We chose

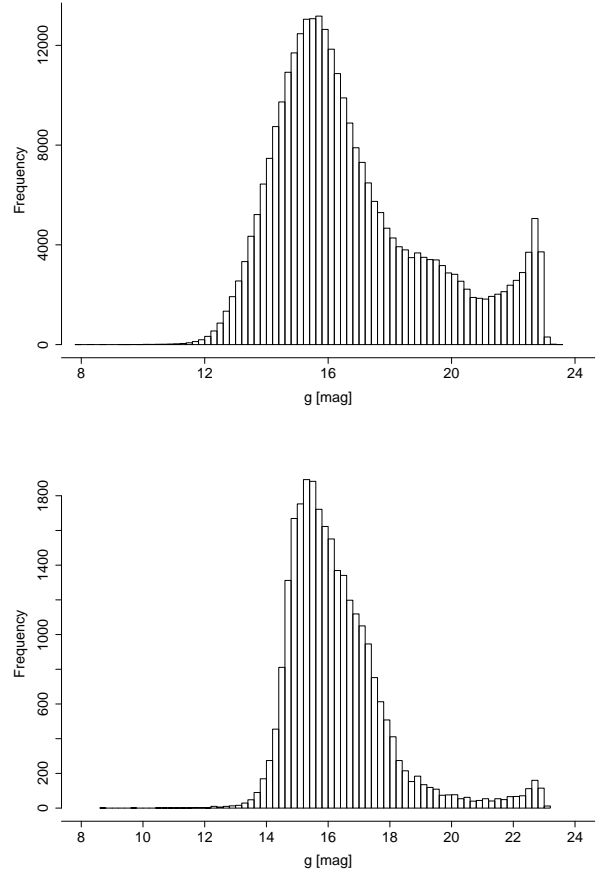


Fig. 15. (Top) g magnitude distribution of sources from DR7 selected to lie in the same data space as the SVM training data. (Bottom) g magnitude distribution of sources classified as BHB stars.

$\nu = 0.01$ based on this fact, and on a visual inspection of the region of the data space in $u - g$, $g - r$ space occupied by the surviving points.

Filtering the photometry according to consistency with the training set, we were left with 294,652 objects. The distribution of these in g magnitude is shown in Fig. 15 (left hand side).

5.2. Classification

For the classification, we trained a new SVM model using all the available BHB stars, plus an equal number of randomly selected non-BHB stars. The 2d prior probability was used to obtain posterior probabilities, and a threshold of 0.5 was applied to these. With this threshold, 27,074 of the new sample objects were classified as BHB stars. Figure 16 shows the probabilities output from the SVM classifier plotted against the probabilities modified by the 2d prior. The threshold for BHB classification is shown by the horizontal line. The threshold obtained by assuming a prior probability $P(BHB) = 0.32$ for all sources is shown with the vertical line. It can be seen that there are peaks in source density at low and high probability, so that the choice of prior does not dominate the classification. The distribution of classified BHB stars in g magnitude is shown in the right hand side of Fig. 15.

5.2.1. Stability of the probabilities

The training set for the classifier is composed of all the available BHB stars, together with an equal number of non-BHB stars selected at random. This means in practice about one third of the non-BHB stars are included in the training set. The output probabilities, and eventual classifications in many cases, will eventually depend on the exact choice of training data. To quantify the stability of the output probabilities, we performed ten resamplings of the training data and subsequent classifications, and found the standard deviations of the output probabilities.

In Fig. 17 we show a histogram of the standard deviations of the probabilities, and a plot of the standard deviation of the probability for each output sources versus the mean value of the probability obtained. There is a broad peak at about 0.015. The histogram has been truncated at $P = 0.1$.

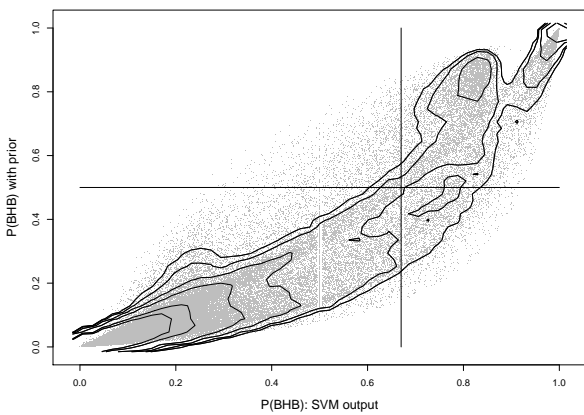


Fig. 16. Classification probabilities $P(\text{BHB})$ for the new sources in the DR7 data set. The abscissa shows the probability returned by the SVM classifier, the ordinate shows the probability after modification with the two dimensional prior (a function of latitude and g magnitude). The horizontal line marks the $P = 0.5$ threshold above which sources were classified as BHB stars for the purposes of this work. The vertical line shows the equivalent threshold for the SVM raw probabilities assuming a simple prior of $P(\text{BHB}) = 0.32$ for all sources. Contours are at 0.004, 0.006, 0.01, 0.03, 0.09 and 0.12 times the maximum density. The highest density regions lie in the bottom left, top right and in the clump at approximately (0.8,0.8).

In Table 6, we show the percentages of objects classified as BHBs or non-BHBs with standard deviation in the probability exceeding 0.01, 0.05 and 0.1. The peak occurs between 0.01 and 0.02 (see also Fig. 17). In each bin, fewer BHB sources than non-BHB sources have higher standard deviations than the given threshold.

It is difficult to combine repeated probabilities into a single value with an uncertainty, and also to include the effect of the magnitude and latitude dependent prior, and we do not attempt to do this. Instead, we give in the output table (Table 7) the raw SVM output probability from one classification, the standard deviation on this from ten resamplings, the prior, and the posterior probability obtained by applying the prior to the raw SVM probability. We use the condition that the posterior probability $P(\text{BHB}) > 0.5$ for BHB classification, but alternatively

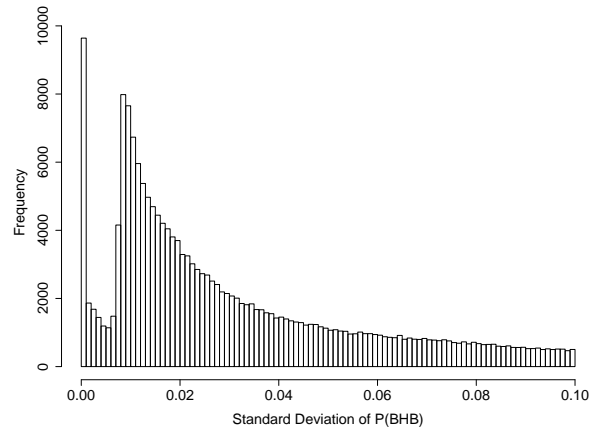


Fig. 17. Histogram of the standard deviations of the probabilities output by the SVM classifier over ten classifications trained on ten separate resamplings of the available training data.

Table 6. Probability standard deviations for BHB and non-BHB classes.

SD >	BHB	non-BHB
0.01	72%	77%
0.02	34%	55%
0.05	16%	29%
0.10	10%	14%

one could impose some condition based on the standard error for each object.

5.3. Photometric distances

Sirko et al. (2004) give absolute g magnitudes based on models by Dorman et al. (1993), for a range of BHB star properties (Teff, $\log g$ and metallicity - their Table 2), together with $u - g$, $g - r$ and $g - i$ colours. To determine photometric distances for our BHB stars, we perform a regression based on this data. We do this with a support vector machine in regression mode*.

We estimate the distance errors due to the uncertainty in the photometry by recomputing the distances with $\pm 1\sigma$ in the colours and in g . the distributions are shown in Fig. 18.

Figure 19 shows the distribution of BHB stars on the sky in the region of the north Galactic cap. The locations of a selection of globular clusters taken from the list of Harris (1996) are shown as black circles. These were used to make a test of the BHB distances, as described below. Also indicated, with a box, is the location of the Ursa Minor dwarf galaxy. The BHB population of this galaxy is clearly visible as a clump of distant stars.

5.4. A distance test

To help assess the accuracy of our BHB identifications and distance determination, we compare our data to a selection of globular clusters taken from the catalogue of Harris (1996) and selected to lie in the north Galactic cap region. Their positions are

* The SVM for regression fits a regression line in a high dimensional feature space, rather than a classification boundary. This involves an extra parameter which must be tuned. For a full description see Drucker et al. (1996) or the libSVM documentation.

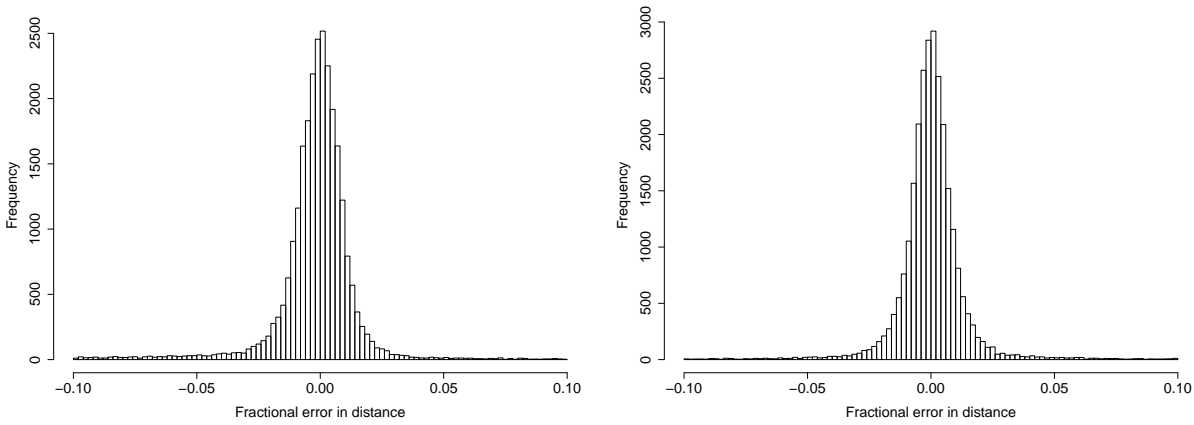


Fig. 18. The fractional change in the derived distance caused by applying a random offset to either the g magnitude or the colours. The offsets are drawn from a Gaussian distribution with the appropriate σ for each object. On the left, the effect of the colour uncertainty on the fitting result, on the right, the effect of the photometric error in g . Both distributions have a width of the same order of magnitude.

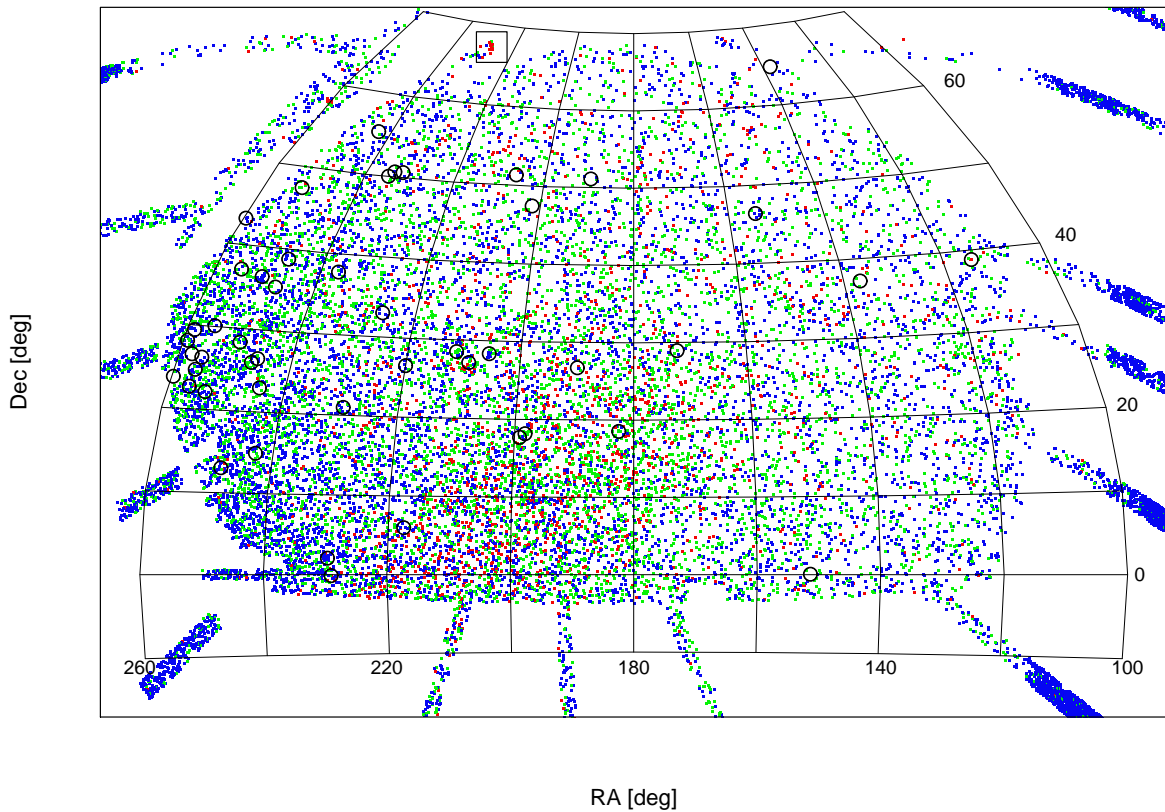


Fig. 19. BHB stars in the north Galactic cap region, shown in Aitoff projection. The stars have been colour coded for distance as follows; blue=closer than 15kpc, green=15-40kpc, red=further than 40kpc. The positions of a few globular clusters selected from the catalogue of Harris (1996) and used for a distance test are shown as black circles. The position of the Ursae Minoris dwarf galaxy is marked with a box.

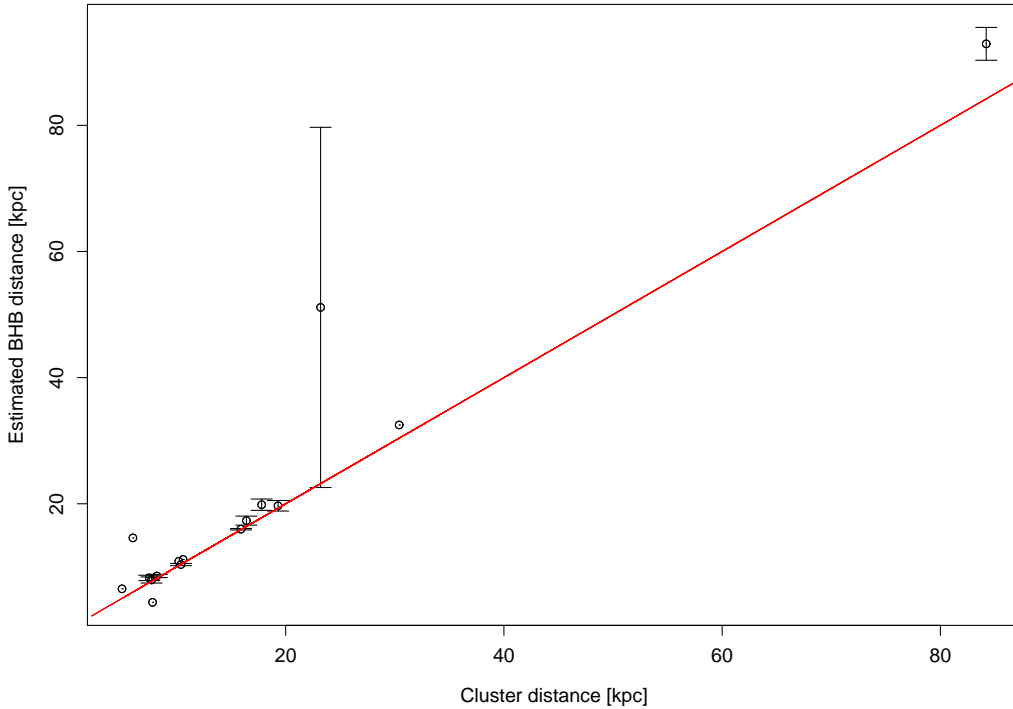


Fig. 20. Distances to globular clusters taken from the catalogue of Harris compared to the mean distance to BHB stars within one tidal radius of the cluster centre (both quantities taken from Harris). The straight line shows exact agreement ($x = y$). Error bars are plotted where possible (> 1 source identified). The main plot shows the full sample, the inset shows the portion closer than 30kpc at a larger scale. Globular clusters with no detected BHB population are not shown.

shown in Fig. 19. We considered all BHB stars within half a tidal radius of each cluster centre to be probable cluster members, and determined the mean distance to those stars, and the error on the mean. We then compare those distances with the ones given in the table of Harris. Out of fifty-two globular clusters within the north Galactic cap region, sixteen had at least one BHB star from our sample within half a tidal radius of the centre. In Fig. 20 is shown the mean distance for each cluster derived from the BHB population compared to the accepted distance given in the catalogue. The agreements with the distances taken from Harris are generally reasonably good for clusters around 20 kpc distant. Amongst the nearby clusters are several with overestimated distances, two of which contain only one source each. Overestimated distances would be expected if the cluster membership is contaminated with non-BHB stars, since the contaminants are generally fainter than the BHB stars and so the distances will be overestimated in those cases. A more distant cluster at just over 80 kpc also has an overestimated distance.

In Fig. 21 we use the information from the globular clusters distance test to further investigate the performance of the classification. We select all sources within half a tidal radius of a cluster centre and calculate the distance to these assuming they are BHB stars (which they will not all be). We then find the fractional absolute residual, R , between this distance, which we call d_* and the accepted cluster distance d_0 ,

$$R = \frac{|d_* - d_0|}{d_0}. \quad (5)$$

We use the absolute residual because the vast majority of sources that have distances inconsistent with the cluster distance are placed on the too distant side (most contaminants will be intrinsically fainter than BHB stars). We plot this against the (prior corrected) SVM probability $P(BHB)$. Sources with $P(BHB) > 0.5$ are classified as BHB stars for the purposes of this plot.

In Fig. 21, sources which are true BHB stars within the cluster should appear close to the cluster distance. We would like to see as many as possible appearing with high probability $P(BHB)$. Sources which are in the cluster but are not BHB stars should be assigned distances greater than the true cluster distance, as they are intrinsically fainter. Ideally, these sources should of course have $P(BHB) < 0.5$. BHB stars that are not genuine cluster members could be in the foreground or the background, so could appear more or less distant than the true cluster distance. Non-BHB stars in the foreground or background could appear at greater or lesser distance than the cluster, but their apparent distance would be greater than their true distance due to their lower luminosity.

We can see in the figure that there is a clump of apparent BHB stars at the cluster distance and with high probability $P(BHB)$. The majority of the sources with incompatible distances for cluster membership also have $P(BHB) < 0.5$. There are a few sources with $P(BHB) > 0.5$ and incompatible distances. These are probably false positive misclassifications, although we cannot rule out the possibility that they are simply foreground or background BHB stars.

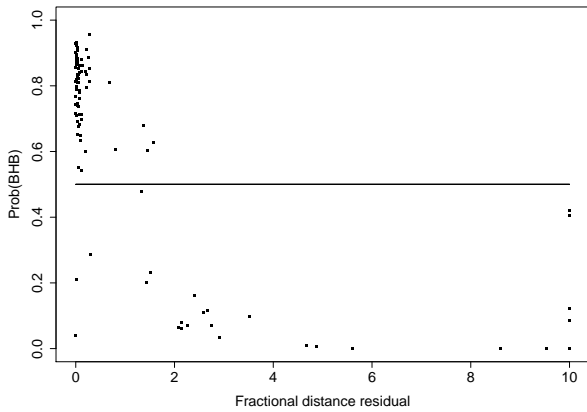


Fig. 21. An analysis of classifier performance based on likely membership of known globular clusters. Sources are selected based on proximity to a known globular cluster from the catalogue of Harris (1996). Distances are computed for all these sources, assuming they are all BHB stars, and compared to the catalogue distance for the cluster. True BHB stars that are really cluster members should return a distance consistent with the cluster distance. Most contaminants from within the cluster will appear too distant compared to the BHB population, because they are fainter. This plot shows the fractional absolute residual in the distance estimate in kpc versus the (prior-corrected) SVM probability $P(BHB)$. The dashed line shows the threshold $P(BHB) = 0.5$.

6. A catalogue of BHB stars from DR7 photometry

In Table 7 we give the basic data for the sample of DR7 sources classified by us. The first four columns of this table show various IDs from SDSS. Column one is the PhotObjId (long) from the SDSS PhotObj table. Columns two to 4 are the plate ID, MJD, and fiber ID for spectroscopic observations (where available) from the SDSS SpecObj table. Columns five to eight are the RA, Dec, l, and b in degrees. Columns nine through thirteen show the SDSS photometry (u, g, r, i, z psfMags). Columns fourteen through eighteen show the errors in the photometry in magnitudes. Columns nineteen through twenty-three show the extinction in each band. Column twenty-four lists the category from Xue et al.. This can be either 'BHB', meaning BHB star from the D0.2 fm method, confirmed by c_γ, b_γ , 'Other', meaning BHB star from D0.2, fm method, rejected by c_γ, b_γ method, 'BS', meaning Blue straggler from D0.2, fm method, 'MS' meaning main sequence star from D0.2, fm method, or 'None' meaning not present in the Xue et al. catalogue. Column twenty-five shows the raw output probability from the SVM. Column twenty-six shows the standard deviation of this probability over ten trials with resampled training set. Column twenty-seven shows the (2d) prior used. Column twenty-eight shows the posterior probability calculated from the SVM probability by applying the prior. Columns twenty-nine and thirty show the assigned distance in kpc and the fractional error.

In the Appendix, we give all the information needed to directly apply the SVM one-class filter and the two-class classifier to new data for which the SDSS colours, $u - g, g - r, r - i$ and $i - z$ are available.

6.1. A warning on extinction

The classification is based on dereddened magnitudes, and the dereddening is performed by the SDSS pipeline based on the map of Schlegel et al. (1998). This is expected to work well at high Galactic latitudes, but for sources in the disk the extinctions may not be reliable. Furthermore, these maps give the line-of-sight extinction to the edge of the Galaxy, so they will underestimate extinction in all cases, possibly by a non-negligible amount even at high latitudes for nearby BHBs.

The catalogue we present contains 181,022 sources with $|b| < 10$ out of the total of 294,652 sources. Out of the probable BHB stars, 7,231 sources have $P(BHB) > 0.5$ and $|b| < 10$, and 19,843 sources have $P(BHB) > 0.5$ and $|b| > 10$. Users should be aware of this issue when considering sources at low Galactic latitude.

To quantify this effect, we calculated the completeness and contamination in the test sample as a function of absolute Galactic latitude. The results are shown in Fig. 22. From this,

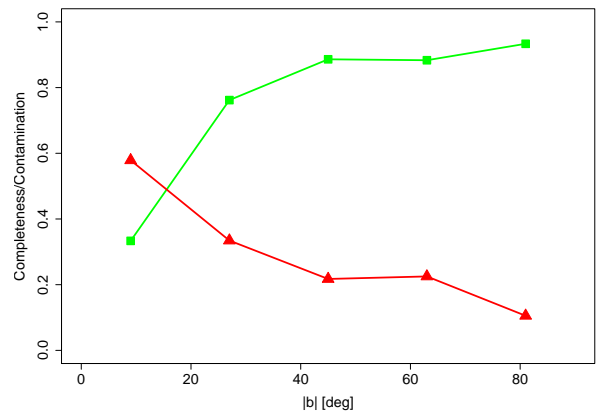


Fig. 22. An analysis of classifier performance on the Xue et al. testing set as a function of absolute Galactic latitude, $|b|$. The completeness (green squares) and contamination (red triangles) are plotted. The sample was restricted to sources with $g < 17.5$. The 2d prior was used, and the contamination is corrected for the likely class fractions.

we can see that the performance of the classifier holds up well for $|b| > 30^\circ$. Below that, there is some degradation, and the performance becomes quite bad in the lowest bin, with $|b| < 18^\circ$. It is difficult to assess the detailed behaviour of the classifier here because of the small number of test sources available (there are 63 sources in the first bin, of which 18 were BHB stars according to Xue et al.).

7. Conclusions

Starting with a sample of spectroscopically identified BHB stars published by Xue et al. (2008), we have trained a number of standard machine learning algorithms to distinguish BHB stars from other contaminating main sequence stars or other interlopers, using SDSS colours alone. We have investigated three methods, with and without the use of probabilistic classification and prior probabilities, and we find that the support vector machine offers the best completeness while simultaneously minimizing

the contamination in the output sample. The kernel density estimator was able to provide comparable contamination, but with a lower completeness. The kNN method was able to match the completeness of the SVM, but not the contamination. Adjusting the classification thresholds altered this picture in various ways, but the SVM generally outperformed the other techniques.

Using the most promising technique (SVM), we have classified a large sample of DR7 data selected to lie within the colour box of Yanny et al. (2000). This sample comprises 859,341 sources. We used a one-class filter (also based on an SVM), to select 294,652 of these as lying in the same colour space as the available training set. We have identified 27,074 of these as probable BHB stars. This includes any already identified by Xue et al. Because our classifier relies on a randomly selected subsample of the available training objects, we ran multiple classifications to quantify the stability of the output probabilities. The standard deviations of the output probabilities are also provided in the table.

We used photometric parallaxes derived from colour data presented in Sirko et al. (2004) to derive distances for these objects, using another variant of the support vector machine to make the fit to the colours. We performed a few simple checks on these distances, and on the spatial distribution of the classified BHB stars, to demonstrate that our method is reasonable.

We include along with this work a catalogue of the 294,652 DR7 sources together with probabilistic identifications as BHB stars, in the hope that these can be useful for other workers either directly as a ready made BHB sample, or as prior probabilities for spectroscopic BHB identification methods. We also provide, in the appendix, the data and parameters necessary to apply our classification to new colour data. The accuracy of the catalogue, or the classifier, can be estimated by reference to the various test results presented in the main body of the paper. In particular, Fig. 12 gives the estimated performance as a function of magnitude, although the reference classifications from the Xue et al. catalogue are unreliable for $g > 19$ as seen from Figs. 2 and 3. Figure 11 gives the expected effect of changing the required threshold probability for BHB classification, whilst Fig. 22 can be used to estimate the performance as a function of Galactic latitude.

A general conclusion of this work is that, where reliable training sets can be identified, machine learning approaches such as those discussed here can probably extract more information than is available with simple colour cuts or *ad hoc* models. This type of approach is likely to be very fruitful in the future for surveys yielding large photometric datasets.

Acknowledgments

The authors would like to thank Vivi Tsalmanza, Jelte de Jong, Connie Rockosi and Hans-Walter Rix for helpful discussions at various stages during the development of this work. We also thank the anonymous referee, whose comments led to significant improvements in the manuscript.

Funding for the SDSS and SDSS-II has been provided by the Alfred P. Sloan Foundation, the Participating Institutions, the National Science Foundation, the U.S. Department of Energy, the National Aeronautics and Space Administration, the Japanese Monbukagakusho, the Max Planck Society, and the Higher Education Funding Council for England. The SDSS Web Site is <http://www.sdss.org/>.

The SDSS is managed by the Astrophysical Research Consortium for the Participating Institutions. The Participating Institutions are the American Museum of Natural History, Astrophysical Institute Potsdam, University of Basel, University of Cambridge, Case Western Reserve University, University of Chicago, Drexel University, Fermilab, the Institute for Advanced Study, the Japan Participation Group, Johns Hopkins University, the Joint Institute for Nuclear Astrophysics, the Kavli Institute for Particle Astrophysics and Cosmology, the Korean Scientist Group, the Chinese Academy of Sciences (LAMOST), Los Alamos National Laboratory, the Max-Planck-Institute for Astronomy (MPIA), the Max-Planck-Institute for Astrophysics (MPA), New Mexico State University, Ohio State University, University of Pittsburgh, University of Portsmouth, Princeton University, the United States Naval Observatory, and the University of Washington.

References

Abazajain K., Adelman-McCarthy J., Agueros M., et al., 2009, *ApJS*, 182, 543
Adelman-McCarthy J., Agueros M., Allam S., et al., 2006, *ApJ*, 162, 38

Bailer-Jones C., Smith K., 2010, Combining probabilities, Tech. Rep. GAIA-C8-TN-MPIA-CBJ-053, URL http://www.mpia-hd.mpg.de/Gaia/publications/probcomb_TN.pdf
Bailer-Jones C., Smith K., Tiede C., et al., 2008, *MNRAS*, 391, 1838
Chang C.C., Lin C.J., 2001
Cortes C., Vapnik V., 1995, *Machine Learning*, 20, 273
Dorman B., Rood R.T., OConnell R.W., 1993, *ApJ*, 419, 596
Drucker H., Burges C., Kaufman L., Smola A., Vapnik V., 1996, In: *NIPS'96*, 155–161
Gao D., Zhang Y.X., Zhao Y.H., 2008, *MNRAS*, 386, 1417
Harrigan M.J., Newberg H.J., Newberg L.A., et al., 2010, *MNRAS*, 621
Harris W., 1996, *AJ*, 112, 1487
Hastie T., Tibshirani R., Friedman J., 2001, *Elements of Statistical Learning*, Springer-Verlag
Hayfield T., Racine J., 2008, *Journal of statistical software*, 27, 1
Huertas-Company M., Tasca L., Rouan D., et al., 2009, *A&A*, 497, 743
Kinman T.D., Morrison H.L., Brown W.R., 2009, *AJ*, 137, 3198
Li Q., Racine J., 2003, *Journal of multivariate analysis*, 86, 266
Marengo M., Sanchez M.C., 2009, *AJ*, 138, 63
Platt J., 1999, In: Smola A., Bartlett P., Schoelkopf D. (eds.) *Advances in large margin classifiers*, MIT press
Richards G., Deo R., Lacy M., et al., 2009a, *AJ*, 137, 3884
Richards G., Myers A., Gray A., et al., 2009b, *ApJS*, 180, 67
Ruhland C., Bell E., Rix H.W., Xue X., 2010, *ApJ*, Submitted
Schlegel D., Finkbeiner D., Davis M., 1998, *ApJ*, 500, 525
Sérsic J., 1968, *Atlas de galaxias australes Cordoba, Argentina: Observatorio Astronomico, Tech. rep.*
Sirko E., Goodman J., Knapp G., et al., 2004, *ApJ*, 127, 899
Tsalmanza P., Kontizas M., Bailer-Jones C., et al., 2007, *A&A*, 470, 761
Tsalmanza P., Kontizas M., Rocca-Volmerange B., et al., 2009, *A&A*, 504, 1071
Vapnik V., 1995, *The Nature of statistical learning theory*, Springer
Xue X., Rix H., Zhao G., et al., 2008, *ApJ*, 684, 1143
Xue X., Rix H., Zhao G., 2009, *Research in Astronomy and Astrophysics*, 9, 1230
Yanny B., Newburg H.J., Kent S., et al., 2000, *ApJ*, 540, 825

Appendix A: Applying the SVM model directly

The application of the SVM model is mathematically straightforward and not excessively laborious. We therefore give here the full specification of the SVM classification so that it can be directly applied to new data.

The input data are the four dereddened SDSS colours $u - g$, $g - r$, $r - i$, $i - z$. The recipe for applying the model consists of five main steps, which are listed below. Below, we give detailed instructions for each step, together with tables containing the necessary model data. The steps are:

1. Apply the one-class model standardization to the data.
2. Evaluate the one-class model and reject outliers.
3. Apply the two-class model standardization to the original data.
4. Apply the two-class model to obtain the decision value, f .
5. Apply the probability model to convert f into $P(BHB)$.

This recipe leaves one with an SVM probability implicitly assuming that BHB stars and non-BHB stars are equal in number in the input sample. An appropriate prior should be applied to obtain the posterior probability.

A.1. Apply the one-class model standardization

The equation for the standardization is

$$\mathbf{x}_s = \frac{\mathbf{x} - \boldsymbol{\mu}}{\sigma}, \quad (\text{A.1})$$

where \mathbf{x} are the colours, $\boldsymbol{\mu}$ are the means and σ the standard deviations of each colour. For the one-class model, the standardization is performed using the one-class values of $\boldsymbol{\mu}$ and σ given in Table A.1.

Table A.1. Standardization parameters for both one-class and two-class classifiers.

	$u - g$	$g - r$	$r - i$	$i - z$
one-class				
μ	1.11589420	-0.11549278	-0.09550841	-0.09199681
σ	0.09485993	0.08260171	0.21371742	0.15484431
two-class				
μ	1.12810095	-0.12914688	-0.10735233	-0.09247437
σ	0.09391075	0.08442376	0.18161768	0.10137230

Table A.2. Parameters for one-class, two-class and probability models.

One-class model

γ	0.25
ρ	2.571136

Two-class model

γ	0.0625
ρ	5.116558

Probability model

A	-1.162976
B	0.006035218

A.2. Application of one-class SVM model

The evaluation equation for the SVM model, for either one-class or two-class classification, is

$$f = \sum_{i=1}^{i=N_s} y_i \alpha_i K(\mathbf{x}, \mathbf{s}_i) - \rho \quad (\text{A.2})$$

where \mathbf{x} is the colour vector to be classified, \mathbf{s}_i are the support vectors, α_i their fitted weights, y_i are class labels for each support vector, and ρ is a constant offset applied to each result. The value of N_s is 152 for the one-class model (Table A.3) and $N_s = 2645$ for the two class model (Table A.4). The class labels y_i are set to +1 or -1 for the two class classifier, and are always set to +1 for the one-class case.

K is a kernel function, in our case an RBF kernel, given by

$$K(\mathbf{x}, \mathbf{s}_i) = \exp(-\gamma \|\mathbf{x} - \mathbf{s}_i\|^2), \quad (\text{A.3})$$

where γ is a parameter found by tuning (Table A.2).

The values of the support vectors for the one-class model, corresponding to the vectors labeled s_i in Equations A.2 and A.3, are given in Table A.3, which is available in its full form as an e-table. The first column in this table gives the product $y_i \alpha_i$ for each vector. The value of the parameters γ and ρ are given in Table A.2.

To apply the one-class model, simply calculate the sum in Equation A.2 over all the support vectors in Table A.3 and subtract the value of ρ . Sources with $f > 0$ are compatible with the training data and are therefore suitable for classification with the two-class classifier. Sources with $f < 0$ are outliers that should be rejected (they cannot be classified with the two-class model).

A.3. Standardization for two-class classification

Having rejected sources not compatible with the model, it is now necessary to standardize the data for the surviving sources using the standardization appropriate for the two-class classifier. The equation for this is identical to that used for the one-class standardization, Equation A.1 above. The parameters are given in Table A.1. Note that this standardization should be performed

Table A.3. Data for the one-class SVM model.

$y_i \alpha_i$	$u - g$	$g - r$	$r - i$	$i - z$
0.177629	-0.125387	-3.43222	2.042456	0.187264
0.853943	-2.771393	-3.613814	0.063207	-0.607082
0.11659	0.665252	0.272304	-1.799065	2.331353
0.388386	0.412248	-0.926218	-0.278366	-3.513227
0.255163	-0.863317	-0.345117	-1.129957	0.309968
1	2.562787	-3.10535	-0.250291	-0.258345
0.382262	-0.958194	0.70813	-1.986228	2.899666
0.281138	-0.515436	-2.064209	-0.535715	-2.544512
1	-1.327159	-1.822084	-2.210824	1.937409

Notes. Only the first ten lines of this table are shown here for illustration, the remainder is available in electronic form. There are a total of 152 support vectors in the online table. Column one is the product $y_i \alpha_i$, columns two to five are the dereddened, standardized colours.

on the *original* dereddened colours, not on the standardized data used for the one-class model.

A.4. Application of the two-class model

The equations for the two-class model are the same as for the one-class, namely A.2 and A.3 above. The data for the model should be taken from Table A.4 (support vectors) and from Table A.2 (model parameters). The decision value y_i in Equation A.2 is now either -1 (non-BHB) or +1 (BHB), but this is of no direct concern to the user since in Table A.4 the value of the product $y_i \alpha_i$ is given.

Evaluate Equation A.2 using the two-class data to obtain the decision value f for each source. Decision values $f > 0$ indicate BHB stars (since the class label for BHB stars is +1) and decision values $f < 0$ indicate non-BHB stars.

A.5. Determine the probability of the classification

If only a classification is required, this step is unnecessary. If a probability is also required, apply the probability model to determine this.

Given the value of the decision value f from step A.4 above, determine the probability by evaluating

$$P(\text{BHB}) = \frac{1}{1 + \exp(Af + B)}, \quad (\text{A.4})$$

where A and B are parameters determined by cross validation during training. The values of these for our model are given in Table A.2.

We note again that this is a 'nominal' probability, assuming equal class fractions in reality, no change in class fraction as a function of position, magnitude, etc. A prior should be introduced to obtain better posterior probabilities, as discussed in Sect. 3.4. The simple prior used in this paper of $P(\text{BHB}) = 0.32$, which roughly accounts for the uneven class fractions, is probably the simplest sensible choice for this.

Table A.4. Data for the two-class SVM model.

$y_i\alpha_i$	$u - g$	$g - r$	$r - i$	$i - z$
1024	0.669775	0.534765	0.034976	0.123055
1024	-1.534446	-1.443351	-0.4881	-0.636521
1024	0.275784	-0.507595	-0.355955	-0.123561
1024	0.584588	0.16757	-0.251339	-0.172884
1024	-0.182098	0.04912	-0.256845	0.192107
1024	-0.352472	-0.957706	-0.543161	-0.212342
1024	-0.586737	0.85458	0.657162	-0.291259
1024	-0.97008	1.340226	0.18364	0.724797
1024	-0.064965	-0.720806	-0.229315	-0.498417

Notes. Only the first ten lines are shown here for illustration. The remainder is available in electronic form. There are a total of 2,645 support vectors in the full online table. The columns have the same meaning as for Table A.3 above. Note that column 1, which gives the product $y_i\alpha_i$, always has the same value for the first ten instances. This is not the case for all the support vectors in the full version.